Novel genetically engineered H3.3G34R model reveals cooperation with ATRX loss in upregulation of *Hoxa* cluster genes and promotion of neuronal lineage

Aalaa S. Abdallah, Herminio J. Cardona, Samantha L. Gadd, Daniel J. Brat, Plamena P. Powla, Waleed S. Alruwalli, Chen Shen, David J. Picketts, Xiao-Nan Li[†], and Oren J. Becher[†]

Department of Pediatrics, Northwestern University, Chicago, Illinois, USA (A.A., X.-N.L., O.J.B.); Stanley Manne Children's Research Institute, Molecular and Translational Cancer Biology, Ann & Robert H. Lurie Children's Hospital of Chicago, Chicago, Illinois, USA (A.A., H.J.C., C.S., X.-N.L., O.J.B.); Department of Pathology, Northwestern University, Chicago, Illinois, USA (S.L.G., D.J.B.); Department of Psychiatry and Behavioral Sciences, Northwestern University , Chicago, Illinois, USA (P.P.P., W.S.A.); Regenerative Medicine Program, Ottawa Hospital Research Institute, Ottawa, Ontario, Canada (D.J.P.); Developmental Therapeutic Core, Robert H. Lurie Comprehensive Cancer Center, Northwestern University Feinberg School of Medicine, Chicago, Illinois, USA (X.-N.L.); Program of Precision Medicine PDOX Modeling of Pediatric Tumors, Ann & Robert H. Lurie Children's Hospital of Chicago, Chicago, Illinois, USA (X.-N.L.); Department of Pediatrics, Kravis Children's Hospital, Icahn School of Medicine at Mount Sinai, New York, New York, USA (O.J.B.); Department of Oncological Sciences, Icahn School of Medicine at Mount Sinai, New York, New York, USA (O.J.B.)

Corresponding Author: Oren J. Becher, MD, Department of Pediatrics, Kravis Children's Hospital, Icahn School of Medicine at Mount Sinai, 1468 Madison Avenue, Annenberg Building A21-10B. New York, NY 10029, USA (oren.becher@mssm.edu).

†Co-senior authors.

Abstract

Background. Pediatric high-grade gliomas (pHGGs) are aggressive pediatric CNS tumors and an important subset are characterized by mutations in *H3F3A*, the gene that encodes Histone H3.3 (H3.3). Substitution of Glycine at position 34 of H3.3 with either Arginine or Valine (H3.3G34R/V), was recently described and characterized in a large cohort of pHGG samples as occurring in 5–20% of pHGGs. Attempts to study the mechanism of H3.3G34R have proven difficult due to the lack of knowledge regarding the cell-of-origin and the requirement for co-occurring mutations for model development. We sought to develop a biologically relevant animal model of pHGG to probe the downstream effects of the H3.3G34R mutation in the context of vital co-occurring mutations.

Methods. We developed a genetically engineered mouse model (GEMM) that incorporates PDGF-A activation, *TP53* loss and the H3.3G34R mutation both in the presence and loss of Alpha thalassemia/mental retardation syndrome X-linked (ATRX), which is commonly mutated in H3.3G34 mutant pHGGs.

Results. We demonstrated that ATRX loss significantly increases tumor latency in the absence of H3.3G34R and inhibits ependymal differentiation in the presence of H3.3G34R. Transcriptomic analysis revealed that ATRX loss in the context of H3.3G34R upregulates *Hoxa* cluster genes. We also found that the H3.3G34R overexpression leads to enrichment of neuronal markers but only in the context of ATRX loss.

Conclusions. This study proposes a mechanism in which ATRX loss is the major contributor to many key transcriptomic changes in H3.3G34R pHGGs.

Accession number. GSE197988.

Key Points

- The RCAS/tv-a system provides an efficient, high-throughput GEMM of H3.3G34R pHGG.
- ATRX loss has a greater effect than H3.3G34R on survival, cell differentiation, and the transcriptome.
- H3.3G34R expression correlates with neuronal lineage in the context of ATRX loss.

Importance of the Study

Biologically relevant animal model systems are critical for the discovery of molecular mechanisms of carcinogenesis. The RCAS/tv-a system provides a fast, high-throughput method to probe region-specific genetic perturbations in an immunocompetent mouse model. Utilizing the RCAS/tv-a system, we have developed several models of pHGGs which incorporate the H3.3G34R mutation either in the presence or absence of ATRX. Our model recapitulates several important molecular and histopathological features of human H3.3G34R pHGGs such as promotion of neuronal lineage and diffusely infiltrating components with perivascular pseudo-rosettes. Our work reveals the critical role ATRX status plays in H3.3G34R mediated gliomagenesis.

Tumors of the central nervous system (CNS) are the most common type of solid tumor of childhood and the leading cause of pediatric cancer deaths.[1,2] Pediatric high-grade gliomas (pHGGs) are among the most aggressive pediatric CNS tumors, with a poor survival rate.[3] A large subset of pHGGs harbor recurrent mutations in histone variant H3.3, namely H3.3K27M and H3.3G34R/V.[4,5] Histone H3.3 is encoded by *H3F3A* and *H3F3B* and are non-canonical as they are deposited onto chromatin independent of the cell cycle. Histone H3.3 is deposited onto both euchromatin and heterochromatin, including at telomeres and pericentric repeats by the ATRX/DAXX complex and H3.3G34 mutant pHGGs almost always contain *ATRX* mutations.[6–8] The recently published inaugural WHO classification of pediatric tumors contains a dedicated section for Pediatric-type diffuse high-grade gliomas defined by H3 status, including the first instance of H3.3G34-mutant pediatric tumors receiving their own official subclassification.[9] Much of the work done to elucidate the effects of H3.3 driver mutations on pHGG tumorigenesis has focused on the H3.3K27M mutation.[9–12] While H3.3K27M and H3.3G34R/V pHGGs have been reported to share many similarities, such as induction of NOTCH pathway genes, H3.3K27M and H3.3G34 mutations are mostly mutually exclusive.[5,13,14] In further contrast to H3.3K27M, H3.3G34 mutations only occur in *H3F3A* and H3.3G34R pHGGs are restricted to the cerebral hemispheres, typically arising in adolescents and young adults.[14]

H3.3G34R-mutant pHGGs almost always co-occur with *TP53* loss and commonly contain PDGFRA amplifications.[14] The mechanism through which the H3.3G34R oncohistone functions during pHGG initiation and progression has not been fully elucidated though it has been continually shown that H3.3G34 mutations impede H3K36 methylation *in cis*, likely through repression of SETD2 activity.[15] Recent *in vitro* studies utilizing immortalized mesenchymal stem cells suggest that H3.3G34R and H3.3G34W, an H3.3G34 mutation found in most of the Giant Cell Tumor of the Bone (GCTB), impedes H3K36 methylation via SETD2 disruption.[16] H3.3G34R/V expression does not appear to have any effect on global H3K27me3 expression and very subtle cell-specific effects; it was separately shown that cells containing H3.3G34L/W mutations are indeed enriched for H3K27me3 at specific loci.[15,17] While there is biochemical justification to believe that mechanisms of H3.3G34 driven tumorigenesis are similar across different organ systems, the exclusivity of particular H3.3G34 mutations to their respective tumor types (H3.3G34W to GCTB and osteosarcoma and H3.3G34R/V to pHGG) necessitates study of these mutations in appropriate model systems.[16–18] Almost all successfully developed GEMMs of H3.3G34 mutant HGGs have incorporated ATRX loss, making it difficult to differentiate between the effects of ATRX status or H3.3G34 mutations on tumorigenesis.

Our objective was to develop a model of pHGG which recapitulates key features of H3.3G34 mutant gliomas and use it to elucidate the role of the H3.3G34R mutation in the context of ATRX status in pHGG initiation and progression. To achieve our objective, we utilized the RCAS/tv-a avian retroviral system to develop a genetically engineered mouse model (GEMM) which incorporates either H3.3WT or H3.3G34R mutant, PDGF-A activation and *TP53* loss, in the context of both ATRX wild-type (WT) and ATRX knockout (KO), thus providing one of the first immunocompetent GEMMs of H3.3G34-mutant pHGG. We found that in our glioma model, overexpression of H3.3G34R does not significantly affect tumor latency or survival relative to overexpression of H3.3WT. We observed that in the absence of H3.3G34R, ATRX loss significantly increases tumor latency and survival but in the presence of H3.3G34R overexpression, ATRX did not significantly impact tumor latency suggesting that the two drivers, ATRX loss and H3.3G34R, cooperate in tumorigenesis. We also found that ATRX loss in the context of H3.3G34R inhibits ependymal differentiation, upregulates *Hoxa* cluster genes, and H3.3G34R overexpression leads to enrichment of neuronal markers but only in the context of ATRX loss.

Materials and Methods

RCAS/tv-a Mouse Modeling

We used the RCAS/tv-a system to overexpress Cre, PDGF-A, and either H3.3G34R-GFP, H3.3WT-GFP or empty vector in two different strains of mice.[19,20] We used the previously described Ntva;p53fl/fl mice[21] and crossed them with ATRX floxed mice generously provided by David Picketts to conditionally delete p53 and ATRX in Nestin+ cells (Ntva;p53fl/fl;ATRXfl/fl).[22] DF1 cells expressing RCAS viruses were injected into the cortex of individual mice from each model between postnatal days 3–5. Injected mice were weighed every other day and monitored daily until tumor symptoms became apparent (20% weight loss, enlarged head, ataxia, seizing or paralysis). Asymptomatic mice were euthanized

after 210 days. Once endpoints were reached, mice were euthanized with CO_2, and brains were removed and either had tumors excised or were fixed with 10% formalin for at least 24 h before embedding in paraffin for histological and immunohistochemical analysis.

Tumor Histology and Immunohistochemistry (IHC)

Formalin-fixed brains (10% formalin for 24 h) were serially sectioned in the coronal plane and processed in paraffin by the Northwestern Mouse Histology and Phenotyping Laboratory. Sections cut at 5-μm were used for histologic and immunohistochemical staining. Hematoxylin and Eosin (H&E) staining were performed using standard protocols. IHC was performed with an automated IHC system (Ventana Medical Systems) with the following antibodies: anti-ATRX (abcam #ab188027, 1:100), anti-GFAP (Cell Signaling Technology #3670S, 1:50), anti-Ki67 (Cell Signaling Technology #12202, 1:400), anti-EMA (Roche Diagnostics, # 05878900001), and anti-Olig2 (Millipore #AB9610, 1:500). IHC was performed using a Vectastain Elite kit (Vector Laboratories #AK-5001) as described previously with the following antibodies: anti-PDGFRA (Cell Signaling Technology, #3174T, 1:1000), anti-pERK1/2 (ABclonal, #AP0472, 1:100), anti-Iba1/AIF-1 (Cell Signaling Technology, #17198T, 1:1500), and anti-H3.3G34R (abcam, #ab254402, 1:1000).[23] Rabbit and mouse antibodies were diluted in 2% BSA solution.

Tumor Histology and Grading

Histologic sections from H3.3G34R and H3.3WT tumors from both ATRX WT and ATRX KO strains were evaluated for infiltration, astroglial or ependymal differentiation, grade, and necrosis. Tumor classification and grading was performed by a neuropathologist blinded to experimental conditions.

RNA-seq Analysis

Total RNA was isolated from snap frozen H3.3WT and H3.3G34R expressing tumors from ATRX WT and ATRX KO mice (n = 5 per group) using the RNeasy kit (Qiagen #74104). Sequencing was performed by the Northwestern University Sequencing Core Facility. The Illumina TruSeq Total RNA Library Preparation Kit (Illumina # 20020596) was used to prepare sequencing libraries including rRNA depletion. Sequencing was performed using an Illumina HiSeq 4000 Sequencer (Illumina) to produce single-end 50-bp reads. Trim Galore (http://www.bioinformatics.babraham.ac.uk/projects/trim_galore/) was used to trim adapters and remove poor quality reads.

Differential Gene Expression

FASTQ files were aligned to the mm10 genome using RNA-STAR, and aligned reads were counted using HTSeq-count with Ensembl mm10 gtf.[24,25] HTSeq-count files were imported into R (https://www.r-project.org/) and differential expression analysis was performed with the DESeq2 package using default settings. DESeq2 normalized reads were imported into GSEA and standard GSEA was run with the following parameters: permutations = 1000, permutation type = gene set, enrichment statistic = weighted, gene ranking metric = signal2noise, max size = 500, min size = 15, normalization mode = meandiv.[26,27] Box plots and volcano plots were generated using the ggplot2 and EnhancedVolcano R packages, respectively.

qRT-PCR Analysis

Total RNA was isolated using the RNeasy kit (Qiagen #74104). cDNA was synthesized from total mRNA using the High-Capacity cDNA Reverse Transcription Kit (ThermoFisher Scientific #4368814). qRT-PCR EasyOligos (Sigma-Aldrich) primers were used for murine *Hoxa2*, *Hoxa3*, *Hoxa4*, *Hoxa5*, *Hoxa7*, *Nefm*, *Nelf* and *Stmn2* (sequences are provided in the Supplementary material). qPCR experiments were run using *Power* SYBR™ Green PCR Master Mix (ThermoFisher Scientific #4367659) on a QuantStudio 6 (ThermoFisher Scientific). Relative gene expression levels were generated using the ddCt method with murine *Taf1c* as the reference gene.

Statistics

Statistical analysis was performed using GraphPad Prism. Survival curves were analyzed using Log-rank (Mantel–Cox) test. Tumor incidence, grade, necrosis, infiltration, and ependymal differentiation were analyzed using Fisher's exact test. IHC data was analyzed using two-tailed unpaired student *t*-tests. *P* values of less than .05 were considered significant for all analyses except DESeq2, in which adjusted *P* values (padj) < .05 were considered significant.

Human pHGG Gene Expression

The raw gene expression count matrix for human cells obtained from a patient harboring pHGG and stably transfected with wild-type H3.3 (n = 4) or H3.3 G34R mutant (n = 3) were downloaded from NCBI GEO (GSE182068).[28] The raw count matrix was imported into DESeq2 for normalization. Genes that satisfied the following criteria were selected for boxplots: (1) significant differential expression in our study and GSE182068 and (2) concordant fold change for G34R vs H3.3 wild-type. Additional human pHGG gene expression data were obtained from the PedcBioPortal (https://pedcbioportal.kidsfirstdrc.org/)[14] for 114 patients with available mRNA expression data and somatic mutation data. H3.3 mutation status was obtained for each patient: H3.3 G34R (n = 10), H3.3 G34V (n = 1), H3.3 K27M (n = 38), and wild-type H3.3 (n = 65). Genes that satisfied the following criteria were selected for boxplots: (1) significant differential expression in our study and (2) concordant fold change for G34R vs all. Boxplots were generated using the normalized log2 expression value (GSE182068) or the z-score (PedcBioPortal).

Study Approval

All experiments with mice were completed in accordance with Northwestern University Center for Comparative Medicine (CCM) guidelines and Institutional Animal Care and Use Committee approved protocols (IACUC, protocol I500005132).

Results

H3.3G34R Overexpression Along with PDGF-A and p53 Loss Induces Tumor Formation Independent of ATRX Status

We infected the frontal cortex of ATRX WT (Nestin TVA; p53$^{fl/fl}$) or ATRX KO (Nestin TVA; p53$^{fl/fl}$; Atrx$^{fl/fl}$) mice with PDGF-A, Cre, and H3.3G34R or H3.3WT and monitored for signs and symptoms of tumor formation (Figure 1A). H3.3G34R expression and reduced ATRX expression were confirmed via IHC (Figure 1B, C and Supplementary Figure 1A). IHC indicated increased expression of pERK1/2 and PDGFRA in tumor bearing mice, a hallmark of PDGFRA overactivation in H3.3G34R tumors (Figure 1D).[29] H&E and Ki67 stained brain tissue sections revealed clusters of proliferating cells or lesions in the brain consistent with tumor formation (Figure 1E). H3.3G34 mutant pHGGs comprise a pathologically heterogenous subset of tumors; our model recapitulated several of these pathological features.[14,30] Most samples were high-grade with diffusely infiltrative and necrotic components and expression of Ki67 and GFAP was present in all groups (Table 1, Figure 1E). It is important to note that Olig2 is highly expressed in most samples in our model despite not being expressed in pHGGs with H3.3G34R in patient samples (Supplementary Figure 1B).

H3.3G34R Overexpression Does not Significantly Impact Tumor Latency or Tumor Incidence Independent of ATRX Status

H&E analysis of ATRX WT H3.3 WT, ATRX WT H3.3G34R, ATRX KO H3.3WT, and ATRX KO H3.3G34R brains revealed tumor incidence of 88%, 81%, 78% and 65%, respectively and there was no significant difference in tumor incidence between any groups (Supplementary Figure 2A). All groups displayed a trend of high-grade tumors; low grade tumors were only observed in H3.3WT injection groups however there was no significant difference in tumor grade between any groups (Figure 2A and Supplementary Figure 2B). We observed no significant difference in overall survival between H3.3WT and H3.3G34R groups independent of ATRX status (Figure 2B).

ATRX Loss Significantly Increases Tumor Latency in the Absence of H3.3G34R Overexpression

ATRX loss significantly increased tumor latency only in the absence of H3.3G34R (Figure 2B). In H3.3G34R expressing mice, ATRX loss increased tumor latency from 90 to 120 days (P = .1, Log-rank test) and in H3.3WT mice, ATRX loss increased tumor latency from 91 to 118 days (P < .01, Log-rank test) (Figure 2B). When comparing H3.3G34R and H3.3WT expressing groups, we observed no difference in survival based on sex for with ATRX KO or ATRX WT animals. However, when comparing ATRX KO to ATRX WT animal survival, we found that females had significantly better survival than males for both H3.3WT expressing (HR = 0.32 [95% CI, 0.15–0.69], Cox regression analysis) and H3.3G34R (HR = 0.46 [95% CI, 0.23–0.92], Cox regression analysis) mice (Supplementary Table 1). Several samples across all 4 groups contained ependymal differentiation as characterized by the presence of perivascular pseudo-rosettes (Table 1). Like H3.3G34-mutant pHGGs, ependymomas are largely GFAP positive and Olig2 negative and so in the absence of molecular profiles, histologic misinterpretation may occur (Figure 2C). Histopathological analysis revealed that ATRX KO H3.3G34R tumors had significantly lower incidence of ependymal differentiation in comparison to ATRX WT H3.3G34R tumors (P < .05, Fisher's exact test), indicating a potential role for ATRX in H3.3G34R tumors on perivascular pseudo-rosette formation (Figure 2C, D). Dot-like immunoreactivity was also observed upon EMA staining (Figure 1E). We did not observe any differences in Iba1 positive myeloid cells between any biological groups (Figure 1F).

ATRX Loss in the Context of H3.3G34R Expression Induces Upregulation of Hoxa Cluster Genes

To elucidate potential mechanisms underlying ATRX mediated differences in overall survival, we extracted tissue from tumors of all 4 groups and performed RNA sequencing (RNA-Seq) analysis (Supplementary Files 1–10). Analysis of tumors from ATRX KO vs ATRX WT mice in H3.3G34R and H3.3WT injection groups indicated significant differential expression of 113 genes and 74 genes, respectively (Supplementary Table 2). Analysis of H3.3G34R vs H3.3WT expressing tumors in ATRX KO and ATRX WT mice indicated significant differential expression of only 34 genes and 12 genes, respectively (Supplementary Table 2). Overall, ATRX status has a greater effect on the tumor transcriptome than the presence of H3.3G34R (Figures 3A and 4B, Supplementary Figure 3). We next performed GSEA analysis to compare the transcriptomes of H3.3WT and H3.3G34R tumors in our ATRX WT and ATRX KO models. ATRX KO H3.3G34R tumors were more enriched for genes associated with "signal metabolic shifts", decreased enrichment of genes associated with "interaction with the extracellular matrix" and "invasiveness" compared to ATRX WT H3.3G34R tumors and ATRX KO H3.3WT tumors displayed increased enrichment of genes associated with "immune/inflammatory signaling" and "NOTCH signaling" as well as decreased enrichment of genes associated with "cell proliferation" and "neuronal markers" compared to ATRX WT H3.3WT tumors (Supplementary Figure 4). Differential expression analysis also revealed upregulation of several *Hoxa* cluster genes (*Hoxa5, Hoxa3, Hoxa7, Hoxa4, and Hoxa2*) and the long-noncoding RNA
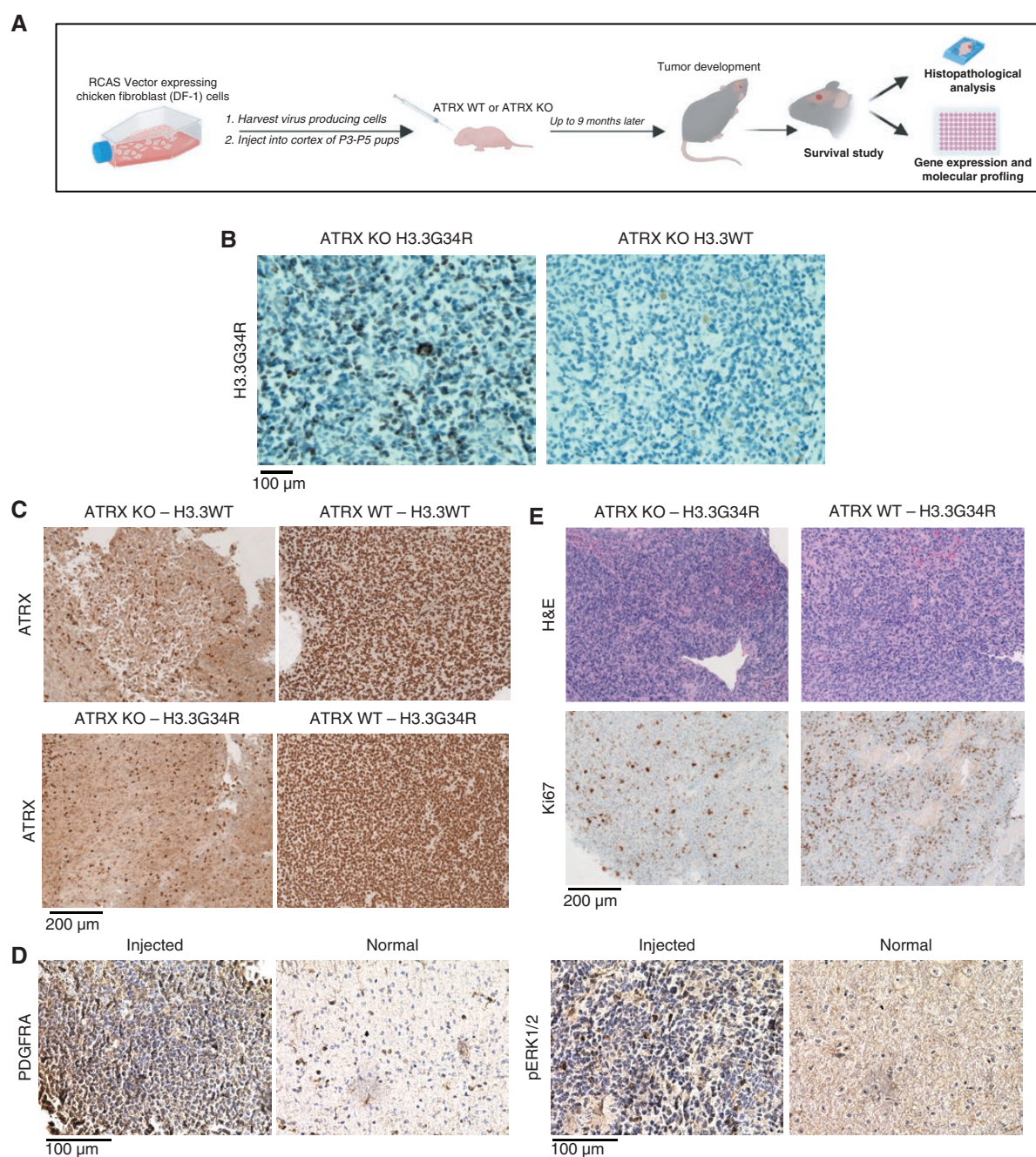
Figure 1. H3.3G34R overexpression along with PDGF-A and p53 loss induces tumor formation independent of ATRX. (A) Development of H3.3G34R and H3.3WT expressing tumors in both ATRX WT and ATRX KO mice using the RCAS/tv-a system workflow. (B) Representative H3.3G34R staining for H3.3G34R and H3.3WT expressing groups. (C) Representative staining for ATRX. (D) Confirmation of PDGFRA overexpression and activation with pERK1/2 as downstream activated kinases in injected RCAS/Ntv-a mice. (E) Representative H&E and Ki67 staining for H3.3G34R-GFP expressing groups.

Hoxaas2 at high levels in ATRX KO H3.3G34R tumors compared to ATRX WT H3.3G34R tumors (Figure 3A, B). The HOXA gene cluster is a critical regulator of both CNS and osteoblast development.[31–33] RT-qPCR confirmed significant upregulation of *Hoxa2, Hoxa3, Hoxa5* and *Hoxa7* in ATRX KO H3.3G34R tumors relative to ATRX WT H3.3G34R tumors (Figure 3C). Interestingly, significant differential expression of *Hoxa* cluster genes was not found in analysis of ATRX KO H3.3WT tumors relative to ATRX WT H3.3WT tumors or in analysis of ATRX KO H3.3G34R tumors relative to ATRX KO H3.3WT tumors (Figure 4B and Supplementary Figure 3).

Table 1. Summary of histopathological analysis of representative tumor samples from all groups

Categories	ATRX KO—H3.3G34R (n=14) (%)	ATRX KO—H3.3WT (n=15) (%)	ATRX WT—H3.3G34R (n=21) (%)	ATRX WT—H3.3WT (n=21) (%)
High/intermediate grade	86	93	100	90
Ependymal differentiation	14	33	62	67
Diffuse infiltration	64	47	33	33
Necrosis	29	53	48	52
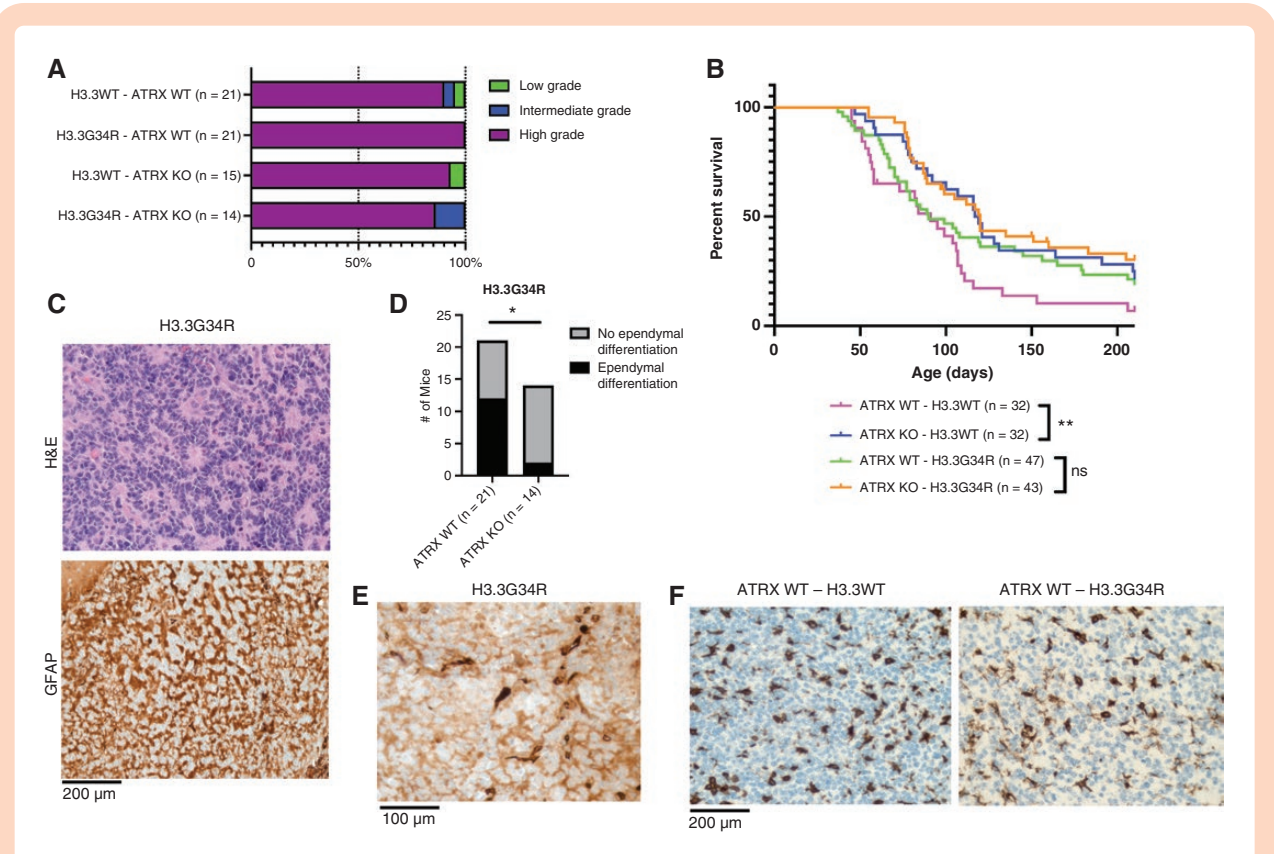
Figure 2. ATRX loss significantly increases tumor latency in the absence of H3.3G34R overexpression. (A) Tumor grades for all injection groups. (B) Kaplan–Meier survival curves for indicated injection groups. (C) Representative GFAP and H&E staining of ependymal differentiation in H3.3G34R-GFP overexpressing samples. (D) Ependymal differentiation incidence for H3.3G34R ATRX WT vs H3.3G34R ATRX KO (*$P < .05$, Fisher's exact test). (E) Representative EMA staining of H3.3G34R-GFP overexpressing samples. (F) Representative Iba1 staining of ATRX WT samples.

H3.3G34R Expression Promotes Neuronal Lineage in the Context of ATRX Loss

GSEA analysis indicated that ATRX KO H3.3G34R tumors have increased expression of genes associated with "cell proliferation" and "metabolism" and decreased expression of genes associated with "interaction with the extracellular matrix" compared to ATRX KO H3.3WT tumors (Supplementary Figure 4). Despite H3.3G34R expression having relatively little effect on the transcriptome of ATRX KO samples, GSEA analysis revealed enrichment of neuronal markers in ATRX KO H3.3G34R vs ATRX KO H3.3WT tumors (Figure 4A). Differential expression data and RT-qPCR confirmed that the neuronal differentiation marker

Stmn2 was significantly upregulated in ATRX KO H3.3G34R vs ATRX KO H3.3WT tumors (Figure 4B, C). Transcriptomic data indicates that *Stmn2* may be upregulated in ATRX KO H3.3G34R samples vs ATRX WT H3.3G34R samples however this difference does not quite reach statistical significance (Figure 4D). *Stmn2* was not upregulated in any other comparison, indicating that H3.3G34R promotes expression of the neural differentiation marker *Stmn2* in the context of ATRX loss (Figure 4B–D). Transcriptomic data indicated that the neurofilament polypeptides, *Nefm* and *Nefl* were significantly upregulated in ATRX KO H3.3G34R samples vs ATRX KO H3.3WT samples and this was confirmed with RT-qPCR (Figure 4B–D). *Nefm* and *Nefl* were not significantly differentially expressed in any other comparison.
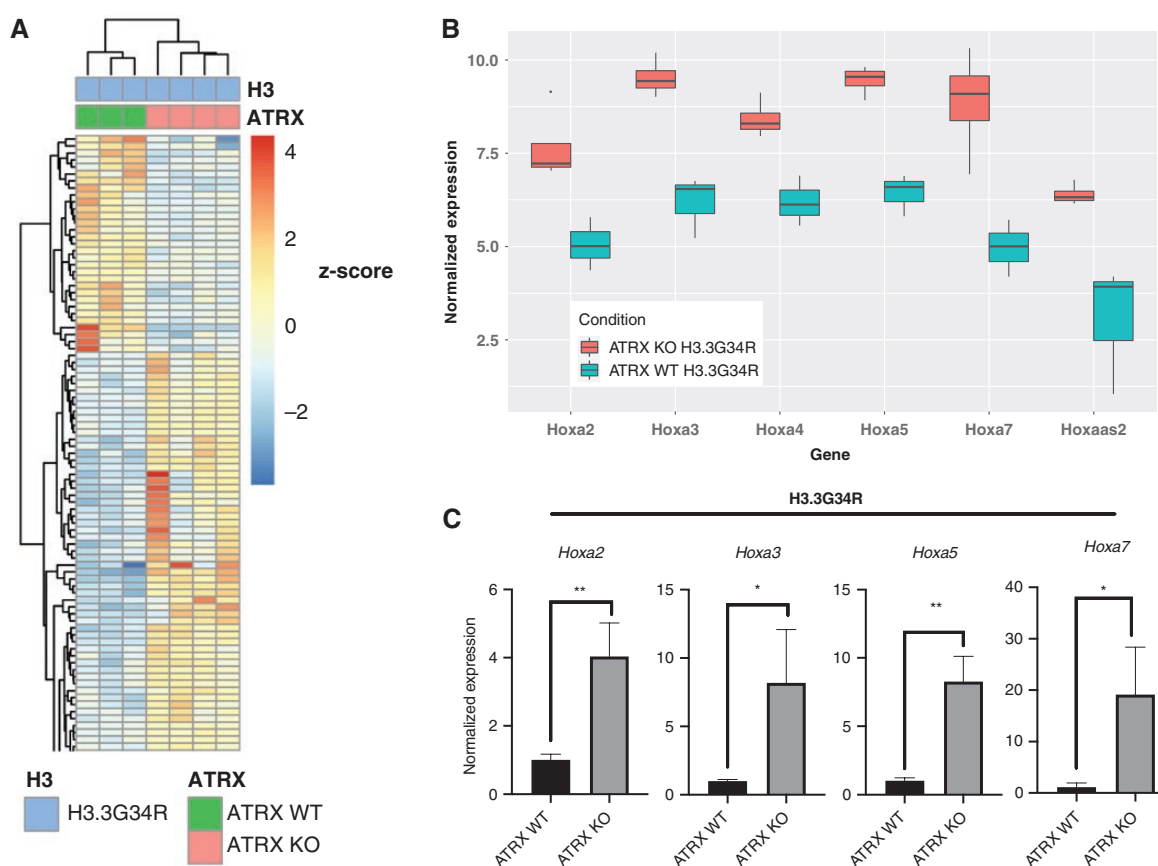
Figure 3. ATRX loss in the context of H3.3G34R induces expression of *Hoxa* genes. (A) Unsupervised hierarchical clustering of differentially regulated genes (padj < .05) in H3.3G34R ATRX WT (n=3) vs H3.3G34R ATRX KO tumors (*n* = 4). (B) Differential expression of *Hoxa* genes (padj < .05) H3.3G34R ATRX WT (n=3) vs H3.3G34R ATRX KO tumors (*n* = 4). (C) RT-qPCR validation of *Hoxa2, Hoxa3, Hoxa5,* and *Hoxa7* upregulation in H3.3G34R ATRX KO vs H3.3G34R ATRX WT tumors (*n* = 3 per group) (*P < .05, **P < .01, two-tailed unpaired *t*-test).

Differential Expression Data from a Murine Model of H3.3G34R Glioma Demonstrates Relevance to the Human Disease

To confirm biological relevance of our novel murine model of H3.3G34R pHGG, we explored whether the 34 genes that were significant differentially expressed between H3.3G34R; ATRX KO and H3.3WT; ATRX KO and the 113 genes that were significantly differentially expressed between H3.3G34R ATRX KO vs ATRX WT were also upregulated in human samples with H3.3G34R. We used one published dataset using an *in vitro* model using a human cell-line, SJ-GBM2, derived from a tumor that developed in a child with a high-grade glioma arising in the cerebral cortex, harboring TP53- and ATRX-inactivating mutations, and stably transfected with H3.3WT or H3.3G34R, and a second dataset of pediatric high-grade glioma samples from the PedcBioPortal that were annotated for H3 status (K27M vs G34R/V vs WT) (Supplementary File 11).[14,28] Out of 34 genes that were significant differentially expressed between H3.3G34R; ATRX KO and H3.3WT; ATRX KO murine tumors in our study, we observed two genes that were significantly differentially expressed

with concordant fold change in the ST-GBM2-H3.3G34R model relative to ST-GBM2-H3.3WT control:COL12A1, and NEFL (Figures 4B and 5A, Supplementary Figure 5).[28] Out of the 113 genes that were significantly differentially expressed between H3.3G34R ATRX KO vs ATRX WT, 13 genes were significantly differentially expressed with concordant fold change in the ST-GBM2-H3.3G34R model relative to ST-GBM2-H3,3WT control: ANPEP, COL6A2, DCT, DPYD, EMC9, HOXA5, HOXA7, LMX1B, MMP3, NCS1, TMEM151A, TMEM130, and VSTM2L (Figures 4B and 5B, Supplementary Figure 5).[28] With regards to the second dataset in PedcBioPortal, none of the 34 genes that were significantly differentially expressed between H3.3G34R; ATRX KO and H3.3WT; ATRX KO murine tumors in our study were concordantly overexpressed in the human G34R mutant tumors relative to the control tumors. Out of the 113 genes that were significantly differentially expressed H3.3G34R ATRX KO vs H3.3G34R ATRX WT, five genes namely, COL5A1, COL6A2, KHDC8A, PDGFD, and PGM5 were concordantly overexpressed in G34R mutant human tumors relative to controls (Figure 3A and 5C).[14] This comparative analysis identified genes for further functional validation in the context of G34R mutant glioma and
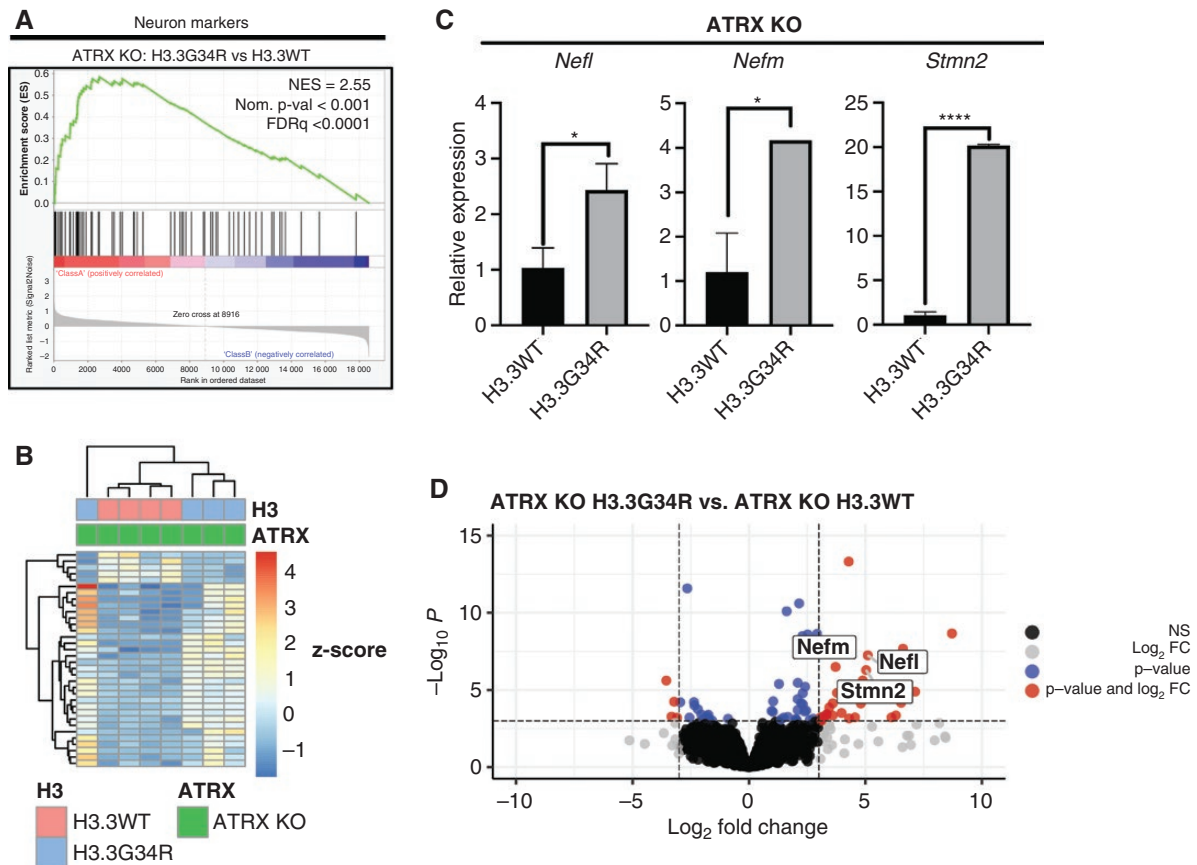
Figure 4.   H3.3G34R expression in the context of ATRX loss promotes neuronal lineage. (A) GSEA plot (FDR < 0.001) of neuron marker activation in H3.3G34R ATRX KO vs H3.3WT ATRX KO tumors ($n = 4$ per group). (B) Unsupervised hierarchical clustering of differentially regulated genes (padj < .05) in H3.3G34R ATRX KO vs H3.3WT ATRX KO tumors ($n = 4$ per group). (C) RT-qPCR validation of *Nefl, Nefm* and *Stmn2* upregulation in H3.3G34R ATRX KO vs ATRX KO H3.3WT tumors ($n = 3$ per group) (*$P < .05$, ****$P < .0001$, two-tailed unpaired *t*-test). (D) Volcano plot highlighting *Stmn2, Nefl,* and *Nefm* upregulation (padj < .05) in H3.3G34R ATRX KO vs H3.3WT ATRX KO tumors ($n = 4$ per group).

supports our observations in the murine model, namely that ATRX loss contributes to the transcriptomal effects of H3.3G34R.

Discussion

Attempts to understand the effects of the H3.3G34R mutation on tumor initiation and progression have increased in the last several years.[29,34,35] Following the identification of recurrent H3.3G34 missense mutations in one of the two genes that encode Histone H3.3 (*H3F3A*), it was postulated that the presence of H3.3G34 mutants decreases SETD2 mediated H3K36 di- and tri- methylation *in cis* however the full mechanism of H3.3G34 mutations on pHGG initiation and progression has not been elucidated.[15,16,18,36] In contrast to the more well-studied H3.3K27M mutation, H3.3G34 pHGGs are a heterogeneous mixture of tumors, making it difficult to develop a robust model. In general, there have been few published H3.3G34R models.[16,29,34,35,37] The first published H3.3G34R mutant glioma model was a patient derived xenograft model (PDX).[13]

Several model systems have been proposed in the last several years and it is only recently that two GEMMs of H3.3G34 gliomas has been developed.[28,29] In one GEMM model, introduction of H3G34R and *TP53* loss via IUE into NPCs of mouse forebrains did not produce any tumors.[11] In a subsequent study with the same IUE method however, they included PDGFRA overexpression, ATRX knockdown, and *TP53* knockout and the resultant mice developed cortical tumors.[29] The same study reported that the majority of human H3.3G34R tumors carry activating *PDGFRA* mutations and that these mutations have high selection pressure during recurrence.[29] Recent work has suggested the H3.3G34R mutation may have a role in tumor initiation but is dispensable for tumor maintenance, further highlighting the need for GEMMs.[16,29,34] In the second GEMM model using Sleeping Beauty Transposase system, H3.3G34R is overexpressed with shRNAs against ATRX and p53 together with a mutant NRAS. The authors apply the model to demonstrate that H3.3G34R impair DNA repair and promote cGAS/STING mediated immune response.[28]

We combined H3.3G34R or H3.3WT overexpression and PDGF-A overexpression with *TP53* and ATRX loss (ATRX
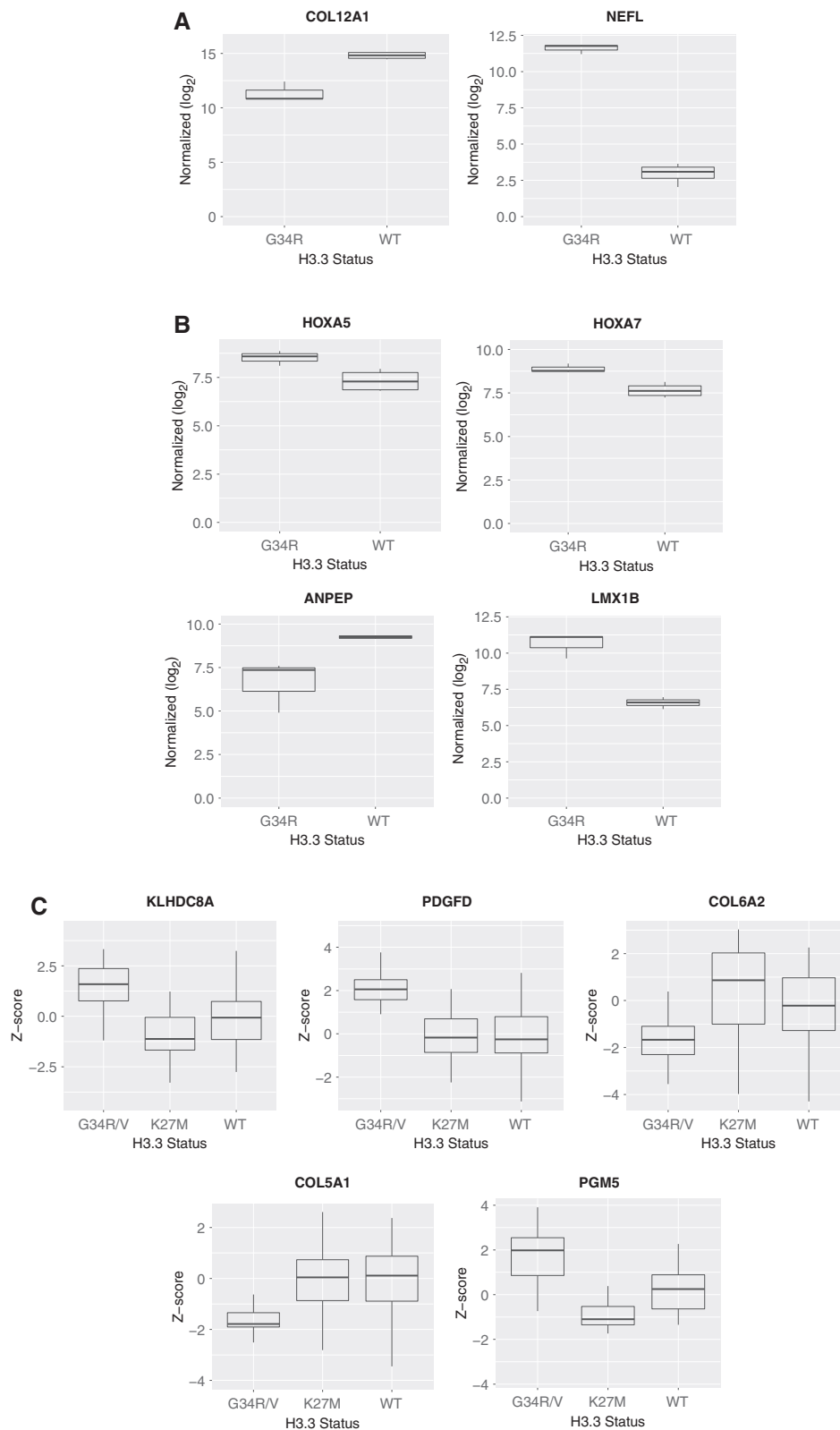
Figure 5. Differential expression data from a murine model of H3.3G34R glioma has similarities to human disease. (A). Box plots for genes which were significantly differentially expressed in the G34R; ATRX KO vs H3.3WT; ATRX KO murine tumors with concordant fold change in the ST-GBM2-H3.3G34R model relative to ST-GBM2-H3.3WT control (padj < .1). (B) Box plots for genes which were significantly differentially expressed in the ATRX KO; G34R vs ATRX WT; G34R murine tumors with concordant fold change in the ST-GBM2-H3.3G34R model relative to ST-GBM2-H3.3WT control (padj < .1) or (C) human G34R mutant tumors relative to K27M mutant tumors and H3WT tumors using the cBioPortal database (padj < .1).

KO) in immunocompetent mice to develop a novel GEMM of H3.3G34R pHGG. While the cell-of-origin for H3.3G34-mutant pHGGs has not been definitively determined, it was previously shown that human fetal neural stem cell (NSC) cultures recapitulate transcriptional signatures of pHGGs indicating a nestin-positive neural stem cell is a candidate cell-of-origin for H3.3G34R pHGGs.[29] Accordingly, we utilized the RCAS/tv-a system to express the H3.3G34R mutation in nestin- expressing progenitor cells of the neonatal murine frontal cortex to model H3.3G34R pHGG *in vivo* and probe potential oncogenic mechanisms of H3.3G34R. In our ATRX KO model, we observed no significant differences in survival between mice overexpressing H3.3G34R vs mice overexpressing H3.3WT; this finding is consistent with earlier work. H3.3G34 mutant gliomas exhibit a trend of increased tumor latency compared to H3.3WT tumors however this trend typically does not reach statistical significance.[38] The majority of H3.3G34 murine models have also reported no significant difference in survival as a result of H3.3G34 expression.[13,16,29,34,35,37] Given the developmental nature of H3.3G34 mutant pHGG, it was suggested that postnatal expression of H3.3G34 mutations in various model systems did not produce meaningful results; however a model in which the G34R/V mutants were introduced into mice embryos mid-gestation via IUE also reported no significant differences in tumor latency or overall survival between groups expressing H3.3G34R/V vs those expressing H3.3WT.[11]

We next chose to focus on the role of ATRX loss in H3.3G34 mutant pHGGs. While *TP53* mutations occur in the majority of H3K27M and H3.3G34R/V pHGGs, ATRX mutations are much more prevalent in H3.3G34 mutant tumors. This result was not entirely surprising as ATRX loss has been associated with better prognosis in other brain tumors.[39] More surprising was the effect the H3.3G34R mutation appeared to have alongside ATRX loss; in the absence of the H3.3G34R mutation, ATRX loss leads to a significant increase in survival and tumor latency, however this effect was not significant when H3.3G34R mutation was expressed. To further elucidate the effect of ATRX loss on H3.3G34R pHGGs, we probed for transcriptomic changes. Overall, we observed that ATRX status had a greater effect on the transcriptome than H3.3G34R presence. Several *Hoxa* genes were upregulated in ATRX KO H3.3G34R mice relative to ATRX WT H3.3G34R mice and not in any other group. RT-qPCR confirmed significant upregulation of murine *Hoxa2*, *Hoxa3*, *Hoxa7*, and *Hoxa5* in ATRX KO H3.3G34R tumors relative to ATRX WT H3.3G34R tumors. Differential gene expression analysis revealed an upregulation of *Hoxa2*, *Hoxa4*, and *Hoxa5* in ATRX KO H3.3G34R relative to ATRX KO H3.3WT tumors though the difference did not quite reach statistical significance. The HOX regulatory genes encode transcription factors and are critical regulators of embryonic development of several organs and cell types includes the CNS and osteoblasts.[31,32] In most vertebrates, the 39 HOX genes are split into four groups or "clusters" including HOXA, HOXB, HOXC and HOXD. In cancer, aberrant expression has been reported for more than half the HOX genes. In the brain, the HOXA cluster has been particularly relevant and is upregulated across various tumor types.[31] The HOXA cluster is located on chromosome 7, which is commonly amplified in GBM though HOXA upregulation has been reported in copy neutral tumors.[33,40–42] H3.3G34R pHGGs are

not described as having chromosome 7 copy number amplifications.[43] We put forth that the enrichment of several *Hoxa* genes is the result of a concerted effort of both ATRX loss and the H3.3G34R mutation. A plausible mechanistic explanation for the synergy is that ATRX is the histone chaperone for H3.3 incorporation onto heterochromatin (with DAXX), or repetitive elements of the genome, such as telomeres while HIRA is the histone chaperone for H3.3 onto euchromatin. It may be that in mice, which harbor longer telomeres, the transcriptomal effects of H3.3G34R are more pronounced when ATRX is deleted, as ATRX deletion, by default, may result in more H3.3G34R becoming incorporated onto euchromatin via HIRA.[6,7,44] Additional studies are required to determine if this potential mechanism is the true reason for the synergy.

While H3K27M pHGGs correlate with mid- to late gestation embryonic expression patterns, transcriptional signatures of H3.3G34R pHGGs typically correlate with early embryonic development.[36] We observed the same trend in our system. We found that H3.3G34R expression upregulates the early neuronal developmental markers *Stmn2, Nefm,* and *Nefl,* but only in the presence of ATRX loss. *Nefm* and *Nefl* are found in the cytoplasm of neurons and are critical components for the development of the neuronal cytoskeleton. Co-expression of *Nefm* and *Nefl* is typically associated with neuron committed progenitors while expression of *Nefm*, *Nefl*, and *Nefh* (the neurofilament triplet) is associated with later stages of neuronal development.[45] *Nefm* and *Nefl* are also commonly used as markers for axonal damage.[45] Given the multiple functions of neurofilament proteins, further work is needed to determine the exact causes of *Nefm* and *Nefl* aberrant expression in ATRX KO H3.3G34R tumor samples as well as resulting phenotypes.

G34R tumors can sometimes present histologically as primitive neuroectodermal tumors (PNET), which are normally comprised of cells observed during early neural development.[46] Single-cell classification of a cohort of adult and pediatric human GBM samples revealed upregulation of *Stmn2* in a molecularly defined cell cluster of what is referred to as neural progenitor (NPC)-like cells.[47] While *Stmn2* plays an important role in neuronal growth, it is also important during early osteogenesis and was recently reported to be differentially regulated in GCTB patient derived H3.3G34W stromal cells.[48,49] This data point provides a potential mechanistic link between H3.3G34R/V pHGG and H3.3G34W/L GCTB/osteosarcoma. Further study is needed to clarify the role of *Stmn2* in both these malignancies.

Comparison of the 34 significantly differentially expressed genes that were significantly upregulated by H3.3G34R relative to H3.3WT in the ATRX KO model to an isogenic human pediatric HGG cell-line that stably expressed H3.3G34R or H3.3WT unraveled 2 genes with concordant overexpression: COL12A1, and NEFL.[28] COL12A1 has not been studied extensively in gliomas but has been implicated in metastasis in breast cancer.[50]

Two potential limitations of our study are (1) loss of *TP53* and/or ATRX as well as expression of H3.3G34R and PDGF-A was induced in mice 3–5 days postnatally and it is unclear when during neural development the H3.3G34 mutation is acquired and (2) Olig2 expression is commonly present in our samples however human pHGG tumor samples are

overwhelmingly Olig2 negative. It was recently proposed that H3.3G34 mutant pHGGs originate in a subset of interneuron progenitors and that the mutated onco-histone somehow keeps its cell-of-origin in an undifferentiated state.[29] OPCs give rise to mature oligodendrocytes (OLs) and DNA methylation data has indicated a lack of activity in genes required for OPC differentiation into OLs in G34 mutant tumors.[29] Potential mechanisms in which H3.3G34 mutations influence preferential differentiations into OLs vs mature inter-neurons (known as the neuron-glial switch) have not been explored. An interneuron progenitor population persists in the SVZ into adulthood therefore, if H3.3G34 mutant pHGGs truly originate in interneuron progenitors, this does not preclude postnatal development of these tumors. Additionally, we were unable to assess the effect of ATRX loss on alternative lengthening of telomeres (ALT) in our ATRX KO samples. While it is known that ATRX loss is not sufficient to induce ALT, the ALT status of this model warrants further study. Our model did in fact recapitulate several histopathological and molecular features of H3.3G34R mutant gliomas despite induction in P3–P5 mouse pups. In summary, our work provides biologically relevant, immunocompetent GEMMs of H3.3G34R pHGG both with and without ATRX loss and highlights the cooperation between H3.3G34R mutations and ATRX loss on *Hoxa* gene activation and neuronal lineage.

Supplementary material

Supplementary material is available online at *Neuro-Oncology Advances* online.

Keywords

ATRX | GEMM | H3.3G34R | HOXA | mouse models | pediatric high-grade glioma | RCAS.

Conflict of interest

The authors declare no potential conflict of interest.

Authorship statement

AA conceived portions of the project, planned and conducted experiments, conducted survival and data analysis and wrote the manuscript. HJC assisted in upkeep of mouse colonies and supervised the project. SLG performed bioinformatics analysis and contributed to the manuscript. DJB performed pathological reviews of tumor models and contributed to data analysis. PPP and WSA assisted in survival analysis and contributed to the manuscript. CS performed mouse crosses and assisted in upkeep of mouse colonies. DJP designed and generated ATRX KO mouse strains. X-NL contributed to the manuscript and secured funding. OJB conceived and supervised the project, secured funding and edited the manuscript.

References

1. Adel Fahmideh M, Scheurer ME. Pediatric brain tumors: descriptive epidemiology, risk factors, and future directions. *Cancer Epidemiol Biomark Prev.* 2021;30(5):813–821.

2. Pollack IF, Jakacki RI. Childhood brain tumors: epidemiology, current management and future directions. *Nat Rev Neurol.* 2011;7(9):495–506.

3. Kasper LH, Baker SJ. Invited Review: emerging functions of histone H3 mutations in paediatric diffuse high-grade gliomas. *Neuropathol Appl Neurobiol.* 2020;46(1):73–85.

4. Wu G, Broniscer A, McEachron TA, et al. Somatic histone H3 alterations in pediatric diffuse intrinsic pontine gliomas and non-brainstem glioblastomas. *Nat Genet.* 2012;44(3):251–253.

5. Schwartzentruber J, Korshunov A, Liu XY, et al. Driver mutations in histone H3.3 and chromatin remodelling genes in paediatric glioblastoma. *Nature.* 2012;482(7384):226–231.

6. Lewis PW, Elsaesser SJ, Noh KM, Stadler SC, Allis CD. Daxx is an H3.3-specific histone chaperone and cooperates with ATRX in replication-independent chromatin assembly at telomeres. *Proc Natl Acad Sci USA.* 2010;107(32):14075–14080.

7. Goldberg AD, Banaszynski LA, Noh KM, et al. Distinct factors control histone variant H3.3 localization at specific genomic regions. *Cell.* 2010;140(5):678–691.

8. Wong LH, McGhie JD, Sim M, et al. ATRX interacts with H3.3 in maintaining telomere structural integrity in pluripotent embryonic stem cells. *Genome Res.* 2010;20(3):351–360.

9. Pfister SM, Reyes-Mugica M, Chan JKC, et al. A summary of the inaugural WHO classification of pediatric tumors: transitioning from the optical into the molecular era. *Cancer Discov.* 2022;12(2):331–355.

10. Larson JD, Kasper LH, Paugh BS, et al. Histone H3.3 K27M accelerates spontaneous brainstem glioma and drives restricted changes in bivalent gene expression. *Cancer Cell.* 2019;35(1):140–155.e7.

11. Pathania M, De Jay N, Maestro N, et al. H3.3(K27M) cooperates with Trp53 loss and PDGFRA gain in mouse embryonic neural progenitor cells to induce invasive high-grade gliomas. *Cancer Cell.* 2017;32(5):684–700.e9.

12. Jones C, Baker SJ. Unique genetic and epigenetic mechanisms driving paediatric diffuse high-grade glioma. *Nat Rev Cancer.* 2014;14(10):651–661.

13. Chen KY, Bush K, Klein RH, et al. Reciprocal H3.3 gene editing identifies K27M and G34R mechanisms in pediatric glioma including NOTCH signaling. *Commun Biol.* 2020;3(1):363.

14. Mackay A, Burford A, Carvalho D, et al. Integrated molecular meta-analysis of 1,000 pediatric high-grade and diffuse intrinsic pontine glioma. *Cancer Cell.* 2017;32(4):520–537.e5.

15. Lewis PW, Muller MM, Koletsky MS, et al. Inhibition of PRC2 activity by a gain-of-function H3 mutation found in pediatric glioblastoma. *Science.* 2013;340(6134):857–861.

16. Jain SU, Khazaei S, Marchione DM, et al. Histone H3.3 G34 mutations promote aberrant PRC2 activity and drive tumor progression. *Proc Natl Acad Sci USA.* 2020;117(44):27354–27364.

17. Shi L, Shi J, Shi X, Li W, Wen H. Histone H3.3 G34 mutations alter histone H3K36 and H3K27 methylation *in cis*. *J Mol Biol.* 2018;430(11):1562–1565.

18. Yang S, Zheng X, Lu C, et al. Molecular basis for oncohistone H3 recognition by SETD2 methyltransferase. *Genes Dev.* 2016;30(14):1611–1616.

19. Holland EC, Varmus HE. Basic fibroblast growth factor induces cell migration and proliferation after glia-specific gene transfer in mice. *Proc Natl Acad Sci USA.* 1998;95(3):1218–1223.

20. Holland EC, Hively WP, DePinho RA, Varmus HE. A constitutively active epidermal growth factor receptor cooperates with disruption of G1 cell-cycle arrest pathways to induce glioma-like lesions in mice. *Genes Dev.* 1998;12(23):3675–3685.

21. Barton KL, Misuraca K, Cordero F, et al. PD-0332991, a CDK4/6 inhibitor, significantly prolongs survival in a genetically engineered mouse model of brainstem glioma. *PLoS One.* 2013;8(10):e77639e77639.

22. Berube NG, Mangelsdorf M, Jagla M, et al. The chromatin-remodeling protein ATRX is critical for neuronal survival during corticogenesis. *J Clin Invest.* 2005;115(2):258–267.

23. Shu Q, Wong KK, Su JM, et al. Direct orthotopic transplantation of fresh surgical specimen preserves CD133+ tumor cells in clinically relevant mouse models of medulloblastoma and glioma. *Stem Cells.* 2008;26(6):1414–1424.

24. Dobin A, Davis CA, Schlesinger F, et al. STAR: ultrafast universal RNA-seq aligner. *Bioinformatics.* 2013;29(1):15–21.

25. Anders S, Pyl PT, Huber W. HTSeq--a Python framework to work with high-throughput sequencing data. *Bioinformatics.* 2015;31(2):166–169.

26. Love MI, Huber W, Anders S. Moderated estimation of fold change and dispersion for RNA-seq data with DESeq2. *Genome Biol.* 2014;15(12):550.

27. Subramanian A, Tamayo P, Mootha VK, et al. Gene set enrichment analysis: a knowledge-based approach for interpreting genome-wide expression profiles. *Proc Natl Acad Sci U A.* 2005;102(43):15545–15550.

28. Haase S, Banerjee K, Mujeeb AA, et al. H3.3-G34 mutations impair DNA repair and promote cGAS/STING-mediated immune responses in pediatric high-grade glioma models. *J Clin Invest.* 2022;132(22):e154229.

29. Chen CCL, Deshmukh S, Jessa S, et al. Histone H3.3G34-mutant interneuron progenitors Co-opt PDGFRA for gliomagenesis. *Cell.* 2020;183(6):1617–1633 e1622.

30. Korshunov A, Capper D, Reuss D, et al. Histologically distinct neuroepithelial tumors with histone 3 G34 mutation are molecularly similar and comprise a single nosologic entity. *Acta Neuropathol.* 2016;131(1):137–146.

31. Céline Gonçalves EsLB, Philippe Arnaud, Bruno Costa. HOX gene cluster (de)regulation in brain: from neurodevelopment to malignant glial tumours. *Cell Mol Life Sci.* 2020;77(19):3797–3821.

32. da Silva RA, Fuhler GM, Janmaat VT, et al. HOXA cluster gene expression during osteoblast differentiation involves epigenetic control. *Bone.* 2019;125:74–86.

33. Cimino PJ, Kim Y, Wu HJ, et al. Increased HOXA5 expression provides a selective advantage for gain of whole chromosome 7 in IDH wild-type glioblastoma. *Genes Dev.* 2018;32(7–8):512–523.

34. Bressan RB, Southgate B, Ferguson KM, et al. Regional identity of human neural stem cells determines oncogenic responses to histone H3.3 mutants. *Cell Stem Cell.* 2021;28(5):877–893.e9.

35. Funato K, Smith RC, Saito Y, Tabar V. Dissecting the impact of regional identity and the oncogenic role of human-specific NOTCH2NL in an hESC model of H3.3G34R-mutant glioma. *Cell Stem Cell.* 2021;28(5):894–905.e7.

36. Sturm D, Witt H, Hovestadt V, et al. Hotspot mutations in H3F3A and IDH1 define distinct epigenetic and biological subgroups of glioblastoma. *Cancer Cell.* 2012;22(4):425–437.

37. Sweha SR, Chung C, Natarajan SK, et al. Epigenetically defined therapeutic targeting in H3.3G34R/V high-grade gliomas. *Sci Transl Med.* 2021;13(615):eabf7860.

38. Korshunov A, Ryzhova M, Hovestadt V, et al. Integrated analysis of pediatric glioblastoma reveals a subset of biologically favorable tumors with associated molecular prognostic markers. *Acta Neuropathol.* 2015;129(5):669–678.

39. Wiestler B, Capper D, Holland-Letz T, et al. ATRX loss refines the classification of anaplastic gliomas and identifies a subgroup of IDH mutant astrocytic tumors with better prognosis. *Acta Neuropathol.* 2013;126(3):443–451.

40. Louis DN, Perry A, Reifenberger G, et al. The 2016 World Health Organization classification of tumors of the central nervous system: a summary. *Acta Neuropathol.* 2016;131(6):803–820.

41. Masui K, Mischel PS, Reifenberger G. Molecular classification of gliomas. *Handb Clin Neurol.* 2016;134:97–120.

42. Gallo M, Ho J, Coutinho FJ, et al. A tumorigenic MLL-homeobox network in human glioblastoma stem cells. *Cancer Res.* 2013;73(1):417–427.

43. Ulgen E, Karacan S, Gerlevik U, et al. Mutations and copy number alterations in IDH wild-type glioblastomas are shaped by different oncogenic mechanisms. *Biomedicines.* 2020;8(12):574.

44. Torne J, Ray-Gallet D, Boyarchuk E, et al. Two HIRA-dependent pathways mediate H3.3 de novo deposition and recycling during transcription. *Nat Struct Mol Biol.* 2020;27(11):1057–1068.

45. Yuan A, Rao MV, Veeranna, Nixon RA. Neurofilaments and neurofilament proteins in health and disease. *Cold Spring Harb Perspect Biol.* 2017;9(4):a018309.

46. Fults D, Pedone CA, Morse HG, Rose JW, McKay RD. Establishment and characterization of a human primitive neuroectodermal tumor cell line from the cerebral hemisphere. *J Neuropathol Exp Neurol.* 1992;51(3):272–280.

47. Neftel C, Laffy J, Filbin MG, et al. An integrative model of cellular states, plasticity, and genetics for glioblastoma. *Cell.* 2019;178(4):835–849.e21.

48. Chiellini C, Grenningloh G, Cochet O, et al. Stathmin-like 2, a developmentally-associated neuronal marker, is expressed and modulated during osteogenesis of human mesenchymal stem cells. *Biochem Biophys Res Commun.* 2008;374(1):64–68.

49. Lutsik P, Baude A, Mancarella D, et al. Globally altered epigenetic landscape and delayed osteogenic differentiation in H3.3-G34W-mutant giant cell tumor of bone. *Nat Commun.* 2020;11(1):5414.

50. Papanicolaou M, Parker AL, Yam M, et al. Temporal profiling of the breast tumour microenvironment reveals collagen XII as a driver of metastasis. *Nat Commun.* 2022;13(1):4587.